International Journal of Computing and Digital Systems
ISSN (2210-142X)
Int. J. Com. Dig. Sys. 3, No.3 (Sep-2014)

A Novel Method for Analysis, Modeling and Simulation of Brushless DC Motors Using MATLAB/SIMULINK

Mahmoud Zadehbagheri[1], Rahim Ildarabadi[2] and Majid Baghaei Nejad[3]

[1' 2' 3]*Faculty of Electrical, Department of Electrical Engineering, Hakim Sabzevari University, Sabzevar ,Iran*

Received 10 Jun. 2014 Revised 20 Jul. 2014, Accepted 15 Aug. 2014, Published 01 Sep. 2014

Abstract: Brushless DC Motors play a significant role in numerous applications. Power density and efficiency are two prominent factors associated with design of these motors. Three phase brushless DC motor is a synchronous permanent magnet motor with rectangular or trapezoidal supply. These motors have a four pole permanent magnet rotors. Stator is a three phase winding supplied by DC voltage. Connecting and disconnecting DC supply depends on the rotor position. For each 30 mechanical degrees of rotor, the supply of windings changes. To detect the position of rotor various methods might be utilized such as hall effect sensor. In this paper a brushless DC Motor is modeled and simulated using MATLAB/SIMULINK.

Keywords: Sensorless Control , Dynamic Performance , Hall Effect Sensors , Brushless DC Motor , Brushless Permanent Magnet Motor

1. INTRODUCTION

Outstanding characteristics of DC motors have increased their application in industry as servo motors; however, they need commutator and brush which, in turn, cause erosion and necessitates periodic repairs. Using solid state switches instead of commutator and brush, has brought about new DC motors called brushless DC motors with diverse telecommunications, electronics and industrial applications [1-3]. Brushless DC motors are similar to synchronous AC motors. But, despite synchronous motors which have sinusoidal counter electromotive force brushless ones generate rectangular or trapezoidal counter electromotive force. Both types of motors have rotating magnetic fields of stator which generates torque in the motor [2-5]. Brushless DC motor is widely applied as low power control motors. Actually, it is not a DC motor but it is a synchronous permanent magnet motor. If this machine is supplied with a source whose frequency is always equal to machine rotor speed it would change to a brushless DC motor. Calling this type of motor as DC does not mean that it is similar to DC motors; yet, it is called DC as its performance characteristics are similar to shunt DC motor with constant field current. The appearance of the system is similar to a three phase permanent magnet synchronous machine. This machine is usually supplied by a six pulse inverter which converts a constant voltage to three phase voltages whose frequency corresponds to instantaneous velocity of rotor. The combination of inverter and machine has characteristics similar to terminal and output characteristics of shunt DC motor. Speed control in this motor is performed using Pulse Width Modulation (PWM) of phase voltages. Phase voltages are alternatively switched to zero [1], [2].

2. THE OPERATION PRINCIPLES OF BLDC MOTORS

In each step of current variation in BLDC motor, one of the stator windings is connected to positive supply via power switches, the second one is connected to negative supply while the third one is left open circuit. Torque is generated as a result of mutual effect between magnetic field, resulted from stator windings, and magnetic field of rotor permanent magnet. Ideally the maximum output torque is achieved when two mentioned fields have 90 degrees phase difference. When the fields move toward each other the generated torque decreases. For thrust force to continue the magnetic field generated by windings must change its position as rotor approaches stator field. A method called "six-level current change" determines supply order of windings.

E-mail address: mzadehbagheri@gmail.com, r.ildar@hsu.ac.ir, mbnejad@hsu.ac.ir

3. SWITCHING SEQUENCE OF POWER DEVICES FOR CHANGING CURRENTS OF STATOR WINDINGS

The undergoing Figure (Figure1) illustrates output signals for Hall effect sensors with respect to counter electromotive force and phase currents.

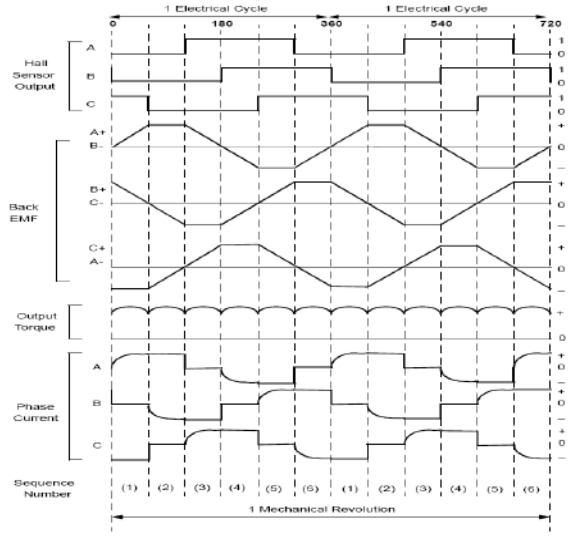

Figure 1. Hall Effect sensors outputs with respect to back EMF and phase currents

Switching combination which must be generated considering the hall sensors conditions.

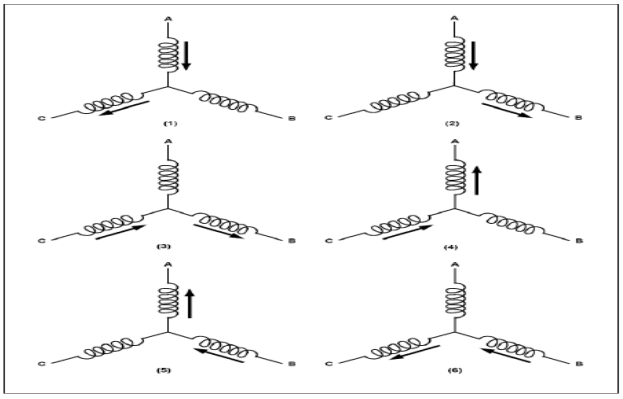

Figure 2. Switching consideration considering Hall effect sensors

It is worth mentioning that the order of numbers in Figure 1 matches numbers shown in Figure 2. At each 60 degrees of electrical rotation (as it has four poles it would be 30 mechanical degrees) one of the Hall effect sensors change their condition. Thus, six steps occur during completion of one electrical cycle. Phase currents switching is performed for each 60 electrical degrees simultaneous with output signals of Hall effect sensors. Anyway, an electrical cycle does not match a complete round of mechanical rotation. The number of electrical cycles which must be completed to obtain a complete mechanical rotation is determined by rotor pole pairs. For each pole pair there would be one electrical cycle in each mechanical round. Therefore, number of electrical cycles in each round of mechanical rotation is equal to number of rotor pole pairs. Figure 3 depicts block diagram of a BLDC motor controller. Q0 to Q5 denote power switches which are switched by a special microcontroller. Based on rated current and voltage of the motor, these switches are selected among MOSFET, IGBT or BJT transistors.

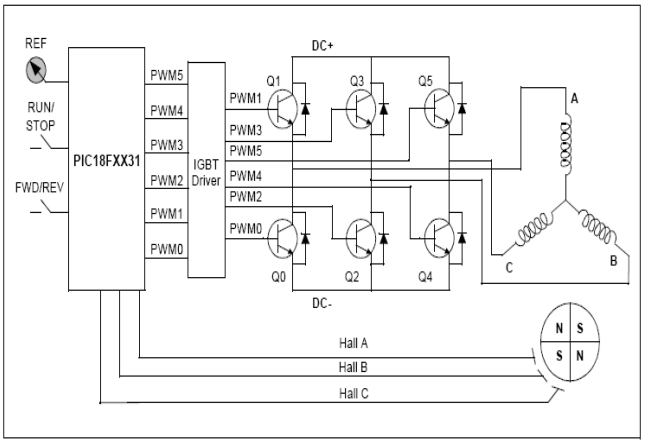

Figure 3. Block diagram of BLDCM controller

4. SENSORLESS CONTROL OF BLDC MOTORS

As mentioned, current of motor windings is changed in accordance with rotor position which is determined by Hall Effect sensors. Nevertheless, current variation of BLDC motors can also be obtained using counter electromotive force instead of Hall sensor effects. As previously said, in each step of current variation one winding is set to positive supply, another one is connected to negative supply and the third one would be open circuit. When counter electromotive force voltage changes from positive to negative or vice versa, output signal of Hall Effect sensor jumps. In ideal conditions, this happens during zero crossing of counter electromotive force; however, there would be time delay due to motor winding characteristics. The time delay is compensated by micro controller. Figure 4 demonstrates block diagram of BLDC motor control system. Since counter electromotive force is proportionate to rotor speed, its amplitude is relatively small in low speed; consequently, zero crossing detection is not possible. Hence, low speed is critical condition which must be noticed. To address this problem, the motor is controlled in open loop manner at the beginning of movement. Subsequently, when the counter electromotive force is large enough, the motor is controlled based on counter electromotive force. The minimum speed, whose counter electromotive force is measurable, might be calculated using counter electromotive force. Obviously, utilizing this method in current changing, Hall Effect sensors could be eliminated which results in simple structure and lower cost. The latter

characteristic is advantage of BLDC motors; because, when motor works in presence of dust and humidity the maintenance of sensors would not be a challenge. Moreover, sensorless control is beneficial if the motor is going to work in hardly accessible places.

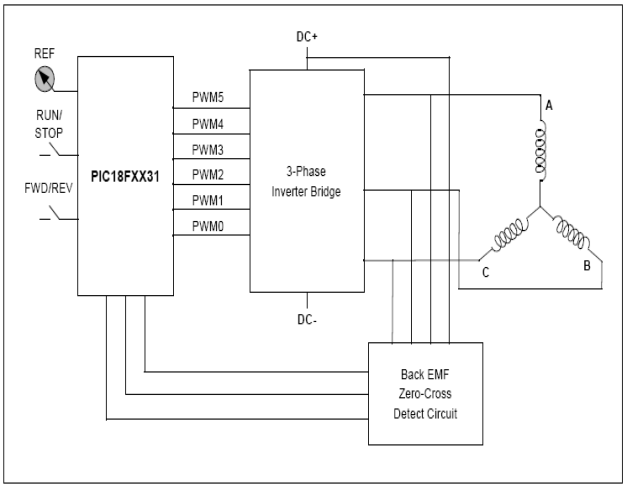

Figure 4. Block diagram of BLDC motor control system

5. MODELING OF BRUSHLESS DC MOTORS

To obtain electrical model of brushless DC machines, numerous equations including lots of constants and variables must be solved. In order to simplify simulations, a few general assumptions are considered which are as follows: the inductance of each phase is considered to be constant during simulation; rotor reluctance is constant with respect to changes of its angles i.e. all poles of the rotor are assumed to be flat; the connection of stator windings is star connection; three phases are balanced; motor moves with its rated speed; there are no damping windings. Considering these assumptions, one may write:

$$\begin{aligned} v_{an} &= R_a i_a + \frac{d}{dt}(L_{aa} i_a + L_{ba} i_b + L_{ca} i_c) + e_a \\ v_{bn} &= R_b i_b + \frac{d}{dt}(L_{ab} i_a + L_{bb} i_b + L_{cb} i_c) + e_b \\ v_{cn} &= R_c i_c + \frac{d}{dt}(L_{ac} i_a + L_{bc} i_b + L_{cc} i_c) + e_c \end{aligned} \quad (1)$$

$$\begin{aligned} R_a &= R_b = R_c = R \\ L_{aa} &= L_{bb} = L_{cc} = L_s \\ L_{ba} &= L_{ab} = L_{ca} = L_{ac} = L_{bc} = L_{cb} = M \end{aligned} \quad (2)$$

The equations of this motor which demonstrate the relation between voltage, current and flux of magnet in the three phase abc system are as follows.

$$\begin{bmatrix} v_a \\ v_b \\ v_c \end{bmatrix} = \begin{bmatrix} R_s & 0 & 0 \\ 0 & R_s & 0 \\ 0 & 0 & R_s \end{bmatrix} \times \begin{bmatrix} i_a \\ i_b \\ i_c \end{bmatrix} + \frac{\partial}{\partial t} \begin{bmatrix} \psi_a \\ \psi_b \\ \psi_c \end{bmatrix} \quad (3)$$

$$\begin{bmatrix} \psi_a \\ \psi_b \\ \psi_c \end{bmatrix} = \begin{bmatrix} L_{aa} & L_{ab} & L_{ac} \\ L_{ba} & L_{bb} & L_{bc} \\ L_{ca} & L_{cb} & L_{cc} \end{bmatrix} \times \begin{bmatrix} i_a \\ i_b \\ i_c \end{bmatrix} + \psi_m \begin{bmatrix} \sin\theta_e \\ \sin(\theta_e - \frac{2\pi}{3}) \\ \sin(\theta_e - \frac{4\pi}{3}) \end{bmatrix}$$

Since the inductance values of the motor are dependent on rotor position and time, solving aforementioned equations is difficult and time consuming. Transforming to rotating reference frame (Park's transformation) is exploited to convert variable coefficients to constant numbers independent of rotor position. In this condition, reference frame rotates with synchronous speed; thus, variable coefficients change to constant ones. Using a proper transformation, three phase equations might be transferred to a two-axis stationary reference frame. Figure.5 presents Vao.Vbo.Vco voltages which are middle point voltages of used DC link for machine terminals. Each phase of motor is demonstrated by armature resistances (Ra.Rb.Rc), inductances (La.Lb.Lc) and counter electromotive forces (Ea.Eb.Ec). Mutual inductances are neglected in this study.

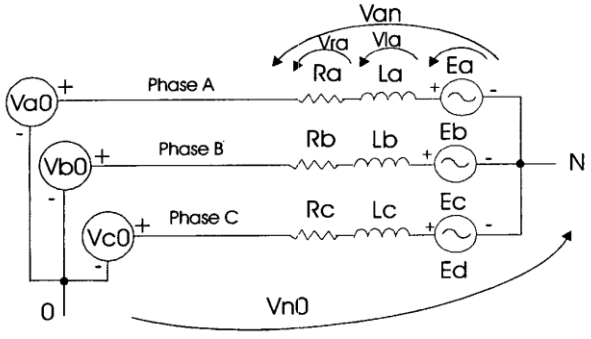

Figure 5. electrical Equivalent circuit of three phase brushless DC Motor

Furthermore, a three phase BLDC motor is known by undergoing equations:

$$\begin{aligned} v_{ab} &= R(i_a - i_b) + L\frac{d}{dt}(i_a - i_b) + e_a - e_b \\ v_{bc} &= R(i_b - i_c) + L\frac{d}{dt}(i_b - i_c) + e_b - e_c \\ v_{ab} &= R(i_c - i_a) + L\frac{d}{dt}(i_c - i_a) + e_c - e_a \\ T_e &= k_f \omega_m + J\frac{d\omega_m}{dt} + T_L \end{aligned} \quad (4)$$

Where back-EMF is calculated using following equations.

$$e_a = \frac{k_e}{2}\omega_m F(\theta_e)$$
$$e_b = \frac{k_e}{2}\omega_m F\left(\theta_e - \frac{2\pi}{3}\right) \quad (5)$$
$$e_c = \frac{k_e}{2}\omega_m F\left(\theta_e + \frac{2\pi}{3}\right)$$
$$T_e = \frac{k_t}{2}\left[F(\theta_e)i_a + F\left(\theta_e - \frac{2\pi}{3}\right)i_b + F\left(\theta_e + \frac{2\pi}{3}\right)i_c\right]$$

F function generates trapezoidal wave.

$$F(\theta_e) = \begin{cases} 1 & 0 \le \theta_e \le \frac{2\pi}{3} \\ 1 - \frac{6}{\pi}\left(\theta_e - \frac{2\pi}{3}\right) & \frac{2\pi}{3} \le \theta_e \le \pi \\ -1 & \pi \le \theta_e \le \frac{5\pi}{3} \\ -1 + \frac{6}{\pi}\left(\theta_e - \frac{5\pi}{3}\right) & \frac{5\pi}{3} \le \theta_e \le 2\pi \end{cases} \quad (6)$$

State space equations of motor could be derived from above equations. Among three voltage and currents one of them is dependent; so, in the equations merely two of them are utilized.

$$i_a + i_b + i_c = 0$$
$$v_{ab} = R(i_a - i_b) + L\frac{d}{dt}(i_a - i_b) + e_a - e_b = 0 \quad (7)$$
$$v_{bc} = R(i_a + 2i_b) + L\frac{d}{dt}(i_a + 2i_b) + e_b - e_c = 0$$

As a result:

$$\begin{pmatrix} i_a' \\ i_b' \\ \omega_m' \\ \theta_m' \end{pmatrix} = \begin{pmatrix} -R/L & 0 & 0 & 0 \\ 0 & -R/L & 0 & 0 \\ 0 & 0 & -k_f/J & 0 \\ 0 & 0 & 1 & 0 \end{pmatrix} \begin{pmatrix} i_a \\ i_b \\ \omega_m \\ \theta_m \end{pmatrix} + \begin{pmatrix} 2/3L & 1/3L & 0 \\ -1/3L & 2/3L & 0 \\ 0 & 0 & 1/J \\ 0 & 0 & 0 \end{pmatrix} \begin{pmatrix} v_{ab} - e_{ab} \\ v_{bc} - e_{bc} \\ T_e - T_L \end{pmatrix} \quad (8)$$

$$\begin{pmatrix} i_a \\ i_b \\ i_c \\ \omega_m \\ \theta_m \end{pmatrix} = \begin{pmatrix} 1 & 0 & 0 & 0 \\ 0 & 1 & 0 & 0 \\ -1 & -1 & 0 & 0 \\ 0 & 0 & 1 & 0 \\ 0 & 0 & 0 & 1 \end{pmatrix} \begin{pmatrix} i_a \\ i_b \\ \omega_m \\ \theta_m \end{pmatrix}$$

6. Simulation of Brushless DC Motor

Figure 6 illustrates generic view of brushless DC motor control system. It consists of motor, six-pulse inverter, hall sensor and its decoder, inverter switch fire command generator and PI controller. The existing model in Simulink software is utilized for motor and inverter. MOSFET switch with reverse diode is exploited in inverter. Snubber resistance is 5000 Ohms and its capacitance is 1uF.

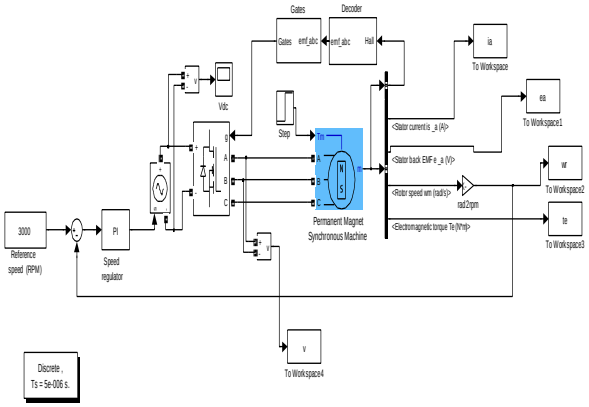

Figure 6. View of Motor control system at the MATLAB environment.

Hall sensor converts rotor position to electrical signal and its operation is implemented through the block shown in Figure 7.

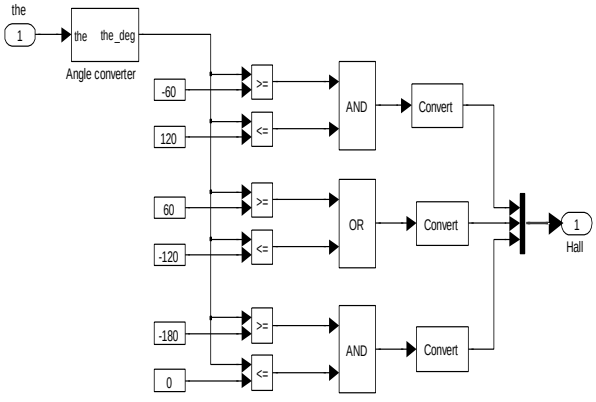

Figure 7. Hall Effect sensor operation

The outputs of sensors are decoded and fed to inverter fire pulse generator. The implementation blocks of these sections are shown in Figures 3 and 4, respectively.

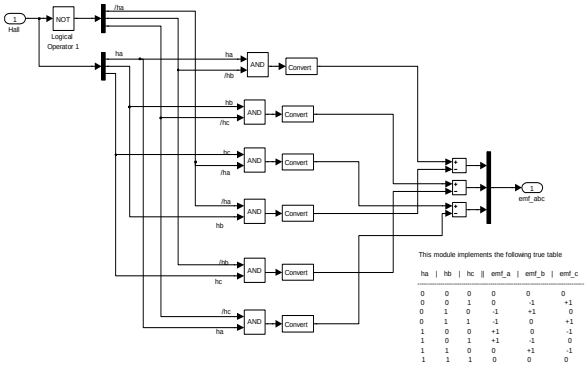

Figure 8. Decoding Hall Effect sensor output

To control the system a PI controller with steady state error cancellation capability is employed. Integrator coefficient is 16.6 and proportional coefficient is 0.013

which are set using trial and error. Figure9 demonstrates this system.

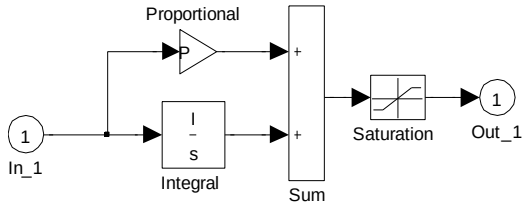

Figure 9. PI controller

In the following a system whose motor is presented in appendix 1 is simulated.

7. SIMULATION OF RESULTS

First off, no load and full load setup conditions are investigated and compared. Figure 10 depicts motor speed during no load starting. It can be seen that motor shows normal operation owing to appropriate controller. Figure 11 demonstrates motor speed during full load setup. As can be seen at the beginning speed experiences a drop and delay as a consequence of load inertia. The beginning of the movement in no load condition is shown in Figure 12 which confirms this issue.

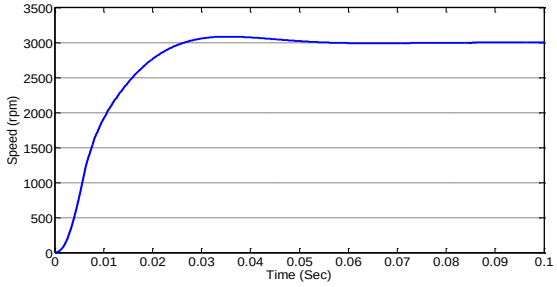

Figure 10. Motor speed during no load starting

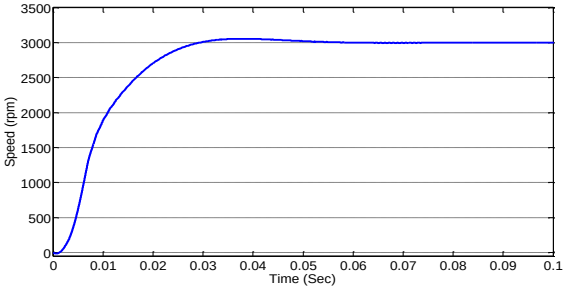

Figure 11. motor speed during full load starting

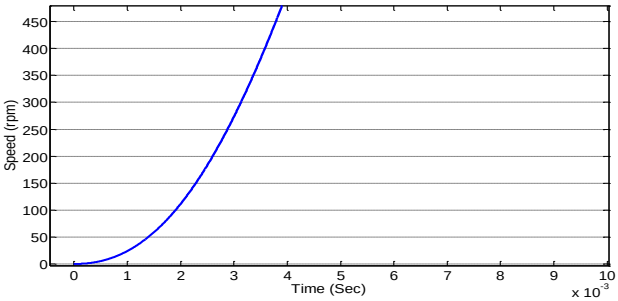

Figure 12. motor speed during no load starting

Torque in these two conditions is shown in Figures 13 and 14, respectively. It is clear that setup torque in full load condition is 5 Nm larger.

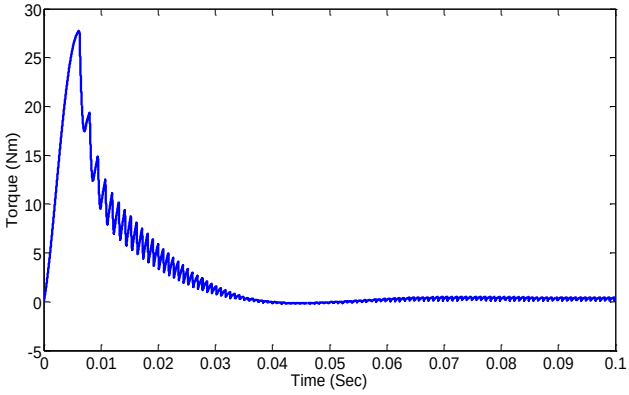

Figure 13. Motor torque during no load starting

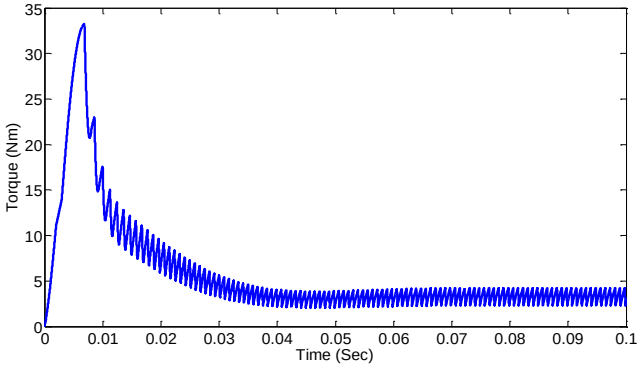

Figure 14. Motor torque during full load starting

Starting currents in these two conditions are depicted in Figures 15 and 16, respectively. As can be seen setup current in full load condition is 4 A larger. Besides, in no load steady state current is almost 0; whereas, in full load condition it is3 A. In the following figures merely phase A current is shown which is sufficient as the phases are balanced.

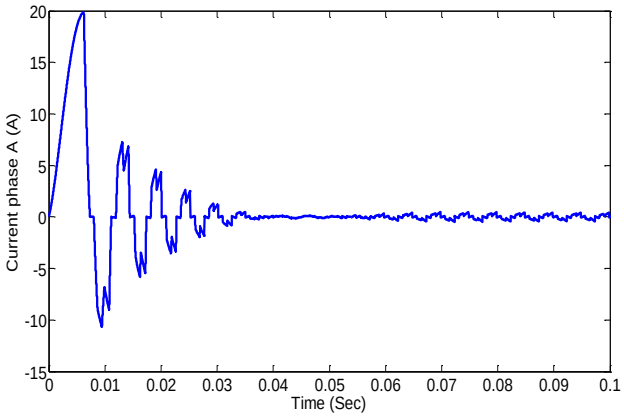

Figure 15. Motor current during no load starting

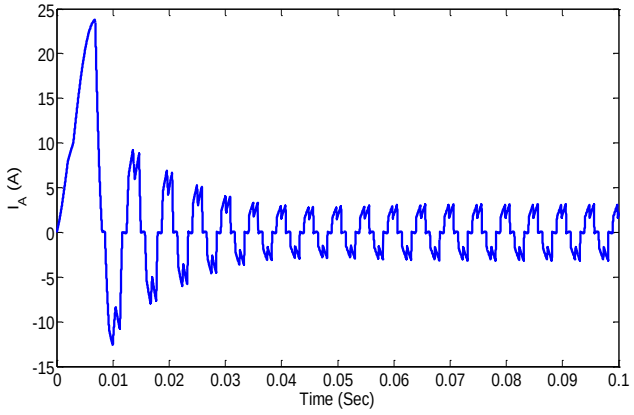

Figure 16. Motor current during full load starting

The voltage of AB line is demonstrated in Figures 17and 18. Additionally, Figures 19 and 20 depict Back-EMF associated with phase A. As shown in the figures line voltage during full load condition is slightly larger while induction voltage is almost the same. It is due to constant flux of permanent magnet.

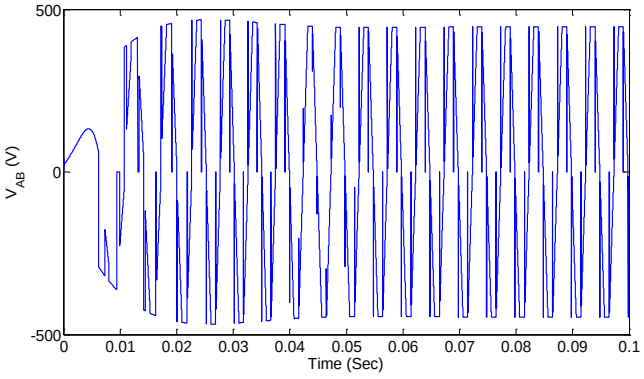

Figure 17. Motor line voltage during no load starting

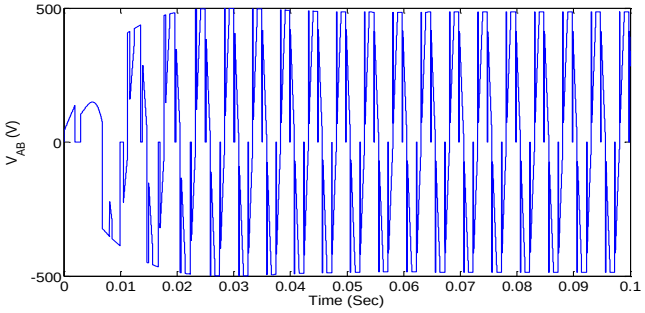

Figure 18. Motor line voltage during full load starting

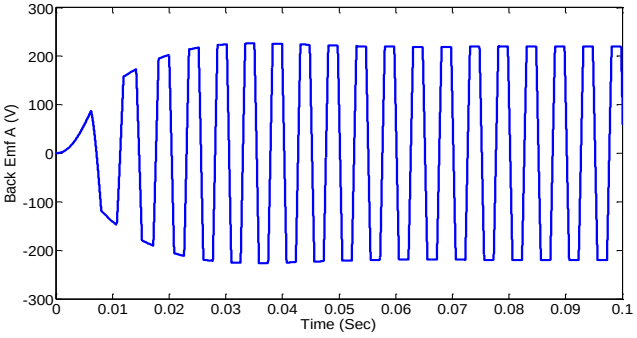

Figure 19. Motor phase induction voltage during no load starting

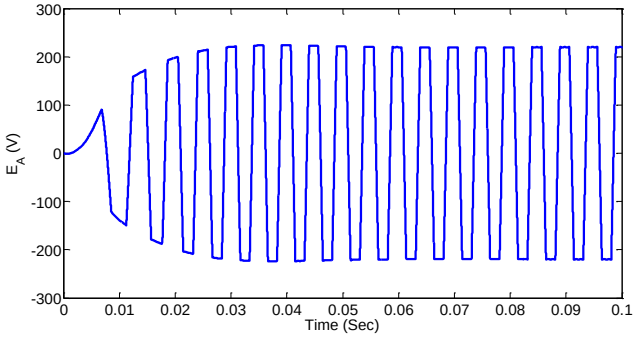

Figure 20. Motor phase induction voltage during full load starting

To achieve engineering perspective Hall sensor output in no load conditions is shown in Figure.21.

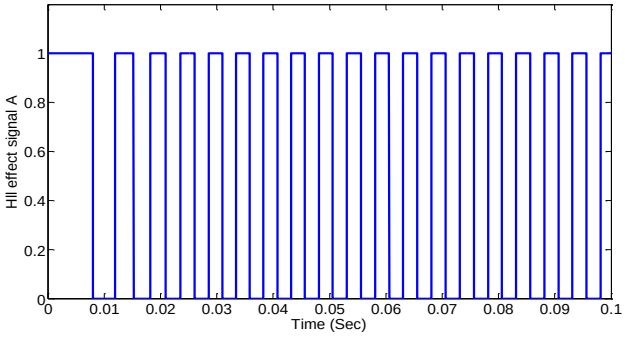

Figure 21. Output signal of motor Hall sensor during no load starting

In the next analyses, applying the load in operating conditions in rated speed is investigated. Motor speed while a 3Nm load is added at t=0.2s is shown in Figure 22. As can be seen, the speed drops 160 rpm and it will be restored. In presence of load, speed curve experiences oscillations depicted in Figure 23. Figure 4 demonstrates the torque when the load is applied. It is evident that oscillation amplitude and motor torque considerably increase. Current of phase A is shown during load application in Figure 25. As expected the current increases.

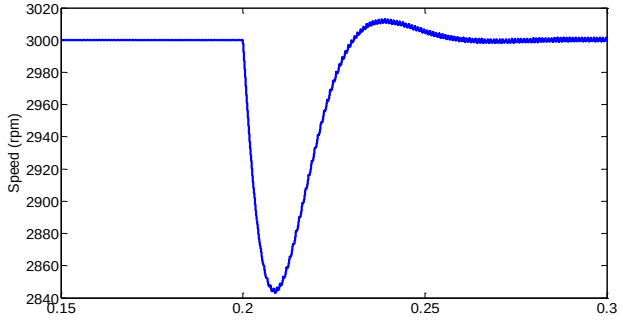

Figure 22. Motor speed when load is applied

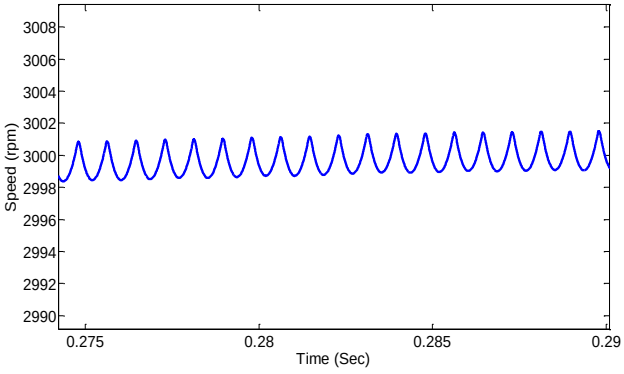

Figure 23. Motor speed oscillations while load is applied

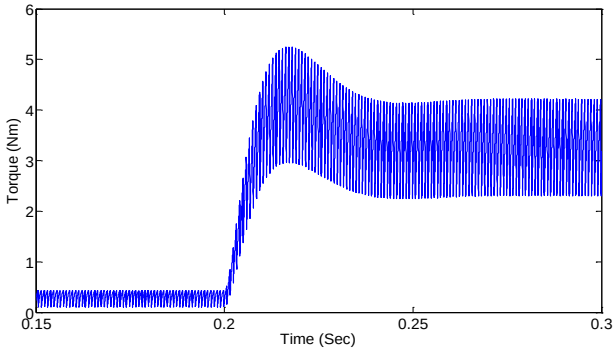

Figure 24. Motor torque while load is applied

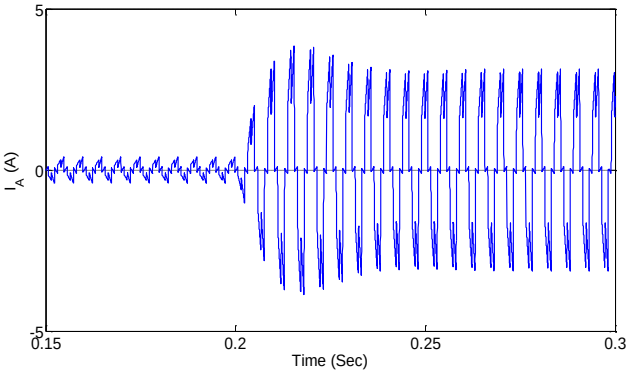

Figure 25. Motor torque while load is applied

Then, the reverse procedure i.e. load reduction is investigated. Speed, torque and current of motor are illustrated in Figures 26-28. Sudden increase in speed, reduction of torque and current and decrease of torque oscillation amplitude are effects of removing the load. Line voltage and induction voltage could be found in figures 29 and 31. During load removal voltage drops slightly but induction voltage is restored after an instantaneous increase resulted from speed increase.

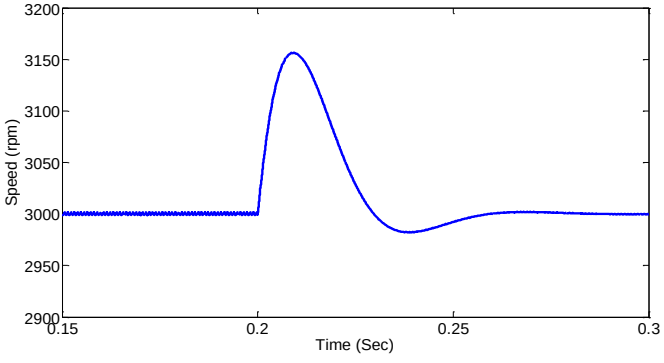

Figure 26. Motor speed during load removal

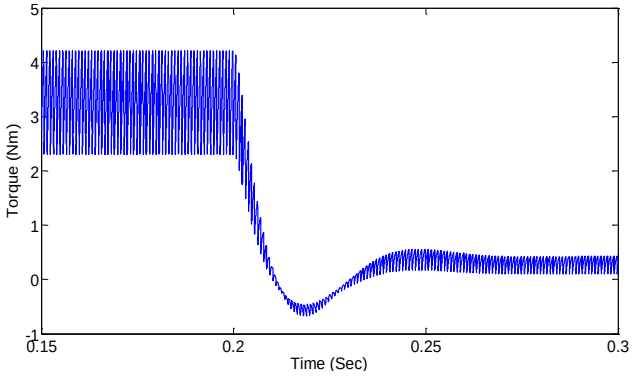

Figure 27. Motor torque during load removal

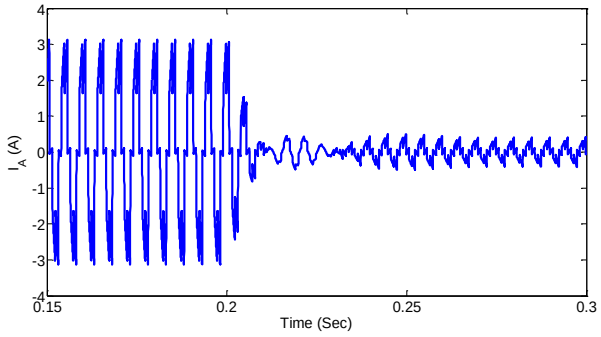

Figure 28. Motor current during load removal

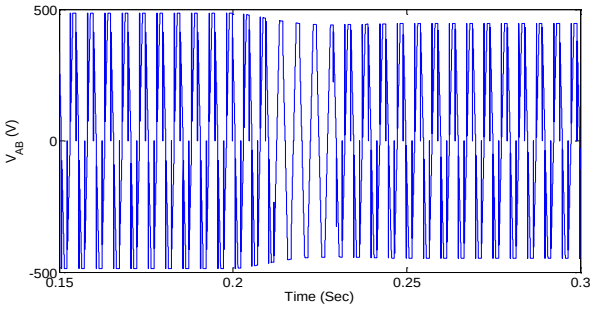

Figure 29. Motor line voltage during load removal

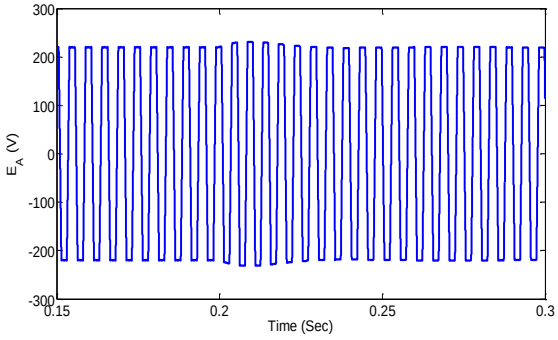

Figure 30. Phase induction voltage of motor during load removal

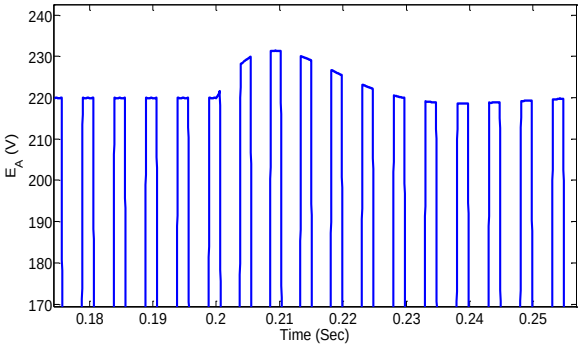

Figure 31. Phase induction voltage of motor during load removal

Finally the effect of changing command speed in the motor is investigated. In Figure 32 it can be seen that speed is decreased from 3000 rpm to 1500 rpm.

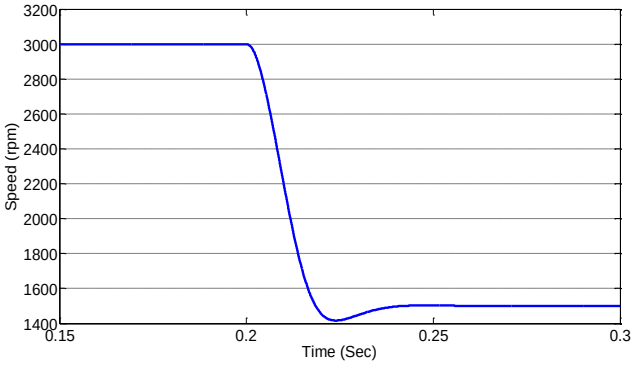

Figure 32. Motor speed during speed command change

8. CONCLUSION

Since copper loss is constant in stimulation winding, conventional DC motors with brush have low efficiency in low speeds. Furthermore weight and volume of such motors encouraged engineers to either provide solutions to deficiencies of these motors or replace them with other electrical machines. An option is brushless DC motor which is a low power control motor with higher efficiency in lower speeds. Moreover, they are lighter. In this paper a Brushless DC motor (BLDCM) was modeled and simulated by MATLAB/SIMULINK. Simulation results revealed the efficiency and performance of the motor.

TABLE I. CHARACTERISTICS OF BRUSHLESS DC MOTOR

P [Pole]	*F [N.m.s]*	*J [kg.m²]*	*Flux [wb]*	*Ls [H]*	*Rs [ohm]*
4	.000103	.0008	.175	8.5e³	2.875

REFERENCES

[1] N Boules,"Two-dimensional field analysis of cylindricalmachines with permanent magnet excitation"IEEE Trans. on Ind., Vol. IA-20, No. 5, Sep 1984J.

[2] Z Q Zhu, D Howe, E Bolte and B Ackermann, "Instantaneous magnetic field distribution inbrushless permanent magnet DC motors, Parts 1-3"IEEE Trans. on Map.. Vol. 29, No. 1, Jan 1993

[3] T W Preston, A B J Reece and P S Sangha"Analysis of switched reluctance drives by thefiniteelementtimestepping method"IEE EMD Conf. No.341, Sept 1991

[4] M.J. Er and B.D.O. Anderson, "Design of reduced-order multirateoutput linear functional observer-based compensator," Automatica, vol.31, no. 2, 1995, pp. 237-242.

[5] S.E. Baek and S.H. Lee, "Design of a multi-rate estimator and itsapplication to a disk drive servo system," Proceedings of 1999American Control Conference, San Diego, CA, June, 1999, pp.3640-3644.

[6] K.L. Moore, S.P. Bhattacharyya and M. Dahleh, "Capabilities andlimitations of multirate control schemes," Automatica, vol. 29, no. 41,1993, pp. 941-95.
[7] B. H. Bae, S. K. Sul, J. H. Kwon, and J. S. Byeon, "Implementation ofsensorless vector control for super-high-speed PMSM of turbo-compressor,"IEEE Trans. Ind. Appl., vol. 39, pp. 811–818, May/Jun. 2003.
[8] L. Zheng, "Design of a superhigh-speed cryogenic permanent magnetsynchronous motor," in Conf. Rec. IEEE Int. Electric Machines andDrive Conf., San Antonio, TX, May 15–18, 2005, pp. 1204–1211.
[9] C. Zwyssig, J. W. Kolar,W. Thaler, and M. Vohrer, "Design of a 100W,500 000 rpm permanent-magnet generator for mesoscale gas turbines,"in Proc. IEEE IAS Ind. Appl. Soc. 40th Annu. Meeting, CD, Oct. 2005.
[10] H. W. Cho, S. M. Jang, and S. K. Choi, "A design approach to reducerotor losses in high-speed permanent magnet machine for turbocompressor,"IEEE Trans. Magn., vol. 42, pp. 3521–3523, Oct. 2006.
[11] R. Krishnan, "Permanent Magnet Synchronous and Brushless DC Motor Drives", CRC Press; 1 edition, 2009.
[12] J.R. Hendershot, T.J.E. Miller,Design of Brushless Permanent-Magnet Machines. Motor Design Books LLC: Second Edition, 2010.
[13] S.A Gholamian, M. Ardebili, K. Abbaszadeh, "Analytic and FEM Evaluation of Power Density for Various Types of Double-Sided Axial Flux Slotted PM Motors", International Journal of Applied Engineering Research, ISSN 0973-4562, vol.3, no.6 , pp. 749–762, 2008.
[14] M. Aydin, S. Huang, T.A Lipo, Optimum design and 3D finite element analysis of nonslotted and slotted internal rotor type axial flux PM disc Machines", IEEE Power Engineering Society Summer Meeting, 15-19 July 2001, vol. 3, pp. 1409 - 1416.
[15] M.Zadehbagheri, R.Ildarabadi, M.baghaei nejad," Sliding Mode Control of a Doubly- fed Induction Generator(DFIG) for Wind Energy Conversion System" International Journal of Scientific & Engineering Research, Volume 4, Issue 11, November-2013 1573,ISSN 2229-5518

Mahmoud Zadehbagheri

was born in Yasouj, Iran in October 1979. In 2003 he received his B.S. in Electrical Engineering from Kashan University and in 2008 he received his M.S. in Electrical Engineering from the Islamic Azad University, Najafabad Branch, he is currently pursuing your PhD at Sabzevar university. He is with the faculty of the Electrical Engineering Department, Islamic Azad University of Yasouj . His research interests includes the fields of power electronics ,electrical machines and drives , FACTS devices and Power Quality.

Rahim Ildarabadi

was born in Sabzevar, Iran in 1975. He received the PhD degree from Ferdowsi University of Mashhad in 2010. He is a full time faculty member at Sabzevar Hkim Sabzevari University. His main area of interest are automation system, electrical machine derive, renewable energy, instruments and measurement. He is currently an Assistant Professor of electrical engineering at Hakim SabzevariUniversity.

Majid Baghaei Nejad

received the B.S. and M.Sc degree in electrical engineering from Ferdowsi University, and Tarbiat Modares University, Iran, in 1996 and 2000 respectively, and his PhD degree in electronic and computer systems from Royal Institute of Technology (KTH), Stockholm, Sweden in 2008. Since 2000 he has been with electronics department at Hakim Sabzevari University, Iran, where currently has an assistance professor position. His current research work includes low power analog/RF integrated circuit design, ultra wideband communication, RFID systems and wireless sensing.